ADVANCED FUNCTIONAL MATERIALS
www.afm-journal.de

Polymer Brush Guided Formation of Conformal, Plasmonic Nanoparticle-Based Electrodes for Microwire Solar Cells

Caroline Sugnaux, Anna Dalmau Mallorquí, Jane Herriman, Harm-Anton Klok, and Anna Fontcuberta i Morral**

This report explores the use of sacrificial thin polymer films prepared by surface-initiated polymerization as a template for the fabrication of highly conformal metal nanoparticle solar cell electrodes. As a first proof-of-principle, the use of this method is demonstrated to prepare top electrodes on planar and microwire-based silicon solar cell devices. These metal nanoparticle films are dual functional in that they not only mediate charge transport, but also enhance light capture due to the plasmonic scattering properties of the nanoparticles. Solar cells with a conformal silver nanoparticle-based electrode layer show short circuit currents that are 46% higher as compared to those exhibit by devices coated with standard indium tin oxide as the electrode. It is anticipated that this methodology will contribute to novel electrode concepts in the next generation solar cells.

1. Introduction

The front electrode is a key element for a large variety of devices, including displays and solar cells. The electrode must maximize light transmission and provide a good electrical conductivity. For a solar cell, it should maximize carrier collection. Traditionally, transparent conductive oxides such as indium tin oxide (ITO) are employed. Novel generations of solar cells include light trapping strategies for the optimization of light absorption while minimizing the amount of material used. These strategies include, e.g., the use of textured top electrodes and films.[1] Along similar lines, recently it has been shown that micro- and nanowires enhance broadband light absorption and ensure minimal material usage for the solar cell.[2–7]

To exploit the full potential of nanowire-based solar cells, a conductive electrode is needed that can be deposited in a conformal manner.[8] Conductive oxides such as ZnO or ITO are one attractive possibility. However, while ITO can be deposited in a relatively conformal manner on nanowires, the scarcity of indium in the earth crust has led researchers to seek alternative solutions. Such alternatives include graphene,[9] carbon nanotubes,[10,11] conductive polymers,[12,13] nanocellulose fiber papers[14] or metal nanowire mesh.[15–18]

While metal nanoarchitectures are potentially interesting electrode materials, their application on complex surfaces, such as, e.g., 3D structured solar cells, is a challenge. This contribution presents a scalable process that allows to fabricate silicon microwire-based solar cells modified with a highly conformal silver or gold nanoparticle film. It will be shown that these metal nanoparticle coatings perform a dual function and not only act as a conductive electrode layer but also enhance light capture due to the fact that the metal nanoparticles behave as plasmonic scattering elements.[19–21] The proposed process is outlined in **Figure 1** and uses an ultrathin coating consisting of densely grafted polymer chains, which are tethered with one chain end to the surface, to guide the formation of a metal nanoparticle-based electrode layer. These surface-grafted polymer films are often colloquially referred to as "polymer brushes." Polymer brush coatings can be fabricated in a bottom-up fashion via surface-initiated polymerization[22] and have already been successfully used as templates for the fabrication of thin inorganic[23–26] and metallic films.[27] Surface-initiated polymerizations are attractive in that they allow to control the thickness of the metal nanoparticle film by controlling the polymer brush thickness and are also compatible with photopatterning strategies, which potentially could allow access to microstructured metal nanoparticle coatings. Furthermore, being a bottom-up strategy, surface-initiated polymerizations also allow facile and controlled deposition of thin, conformal polymer coatings on complex, 3D structured substrates, such as, e.g., nano- or microwires or nano- or microporous materials, which is challenging to achieve using more conventional polymer film forming methods such as spin- or drop-casting. The fabrication of the metal nanoparticle-based electrodes starts with modification of the solar cell surface with an appropriate polymerization initiator, followed by surface-initiated polymerization to generate a thin polymer brush film (Figure 1). In the present work, atom transfer radical polymerization (ATRP) was used to grow the polymer brushes. After that, the polymer

Dr. C. Sugnaux, Prof. H.-A. Klok
École Polytechnique Fédérale de Lausanne (EPFL)
Institut des Matériaux and Institut des Sciences et Ingénierie Chimiques
Laboratoire des Polymères
Bâtiment MXD, Station 12
CH-1015 Lausanne, Switzerland
E-mail: harm-anton.klok@epfl.ch

Dr. A. Dalmau Mallorquí, J. Herriman, Prof. A. Fontcuberta i Morral
École Polytechnique Fédérale de Lausanne (EPFL)
Institut des Matériaux, Laboratoire des Matériaux Semiconducteurs
Bâtiment MXC, Station 12, CH-1015 Lausanne, Switzerland
E-mail: anna.fontcuberta-morral@epfl.ch

DOI: 10.1002/adfm.201404235

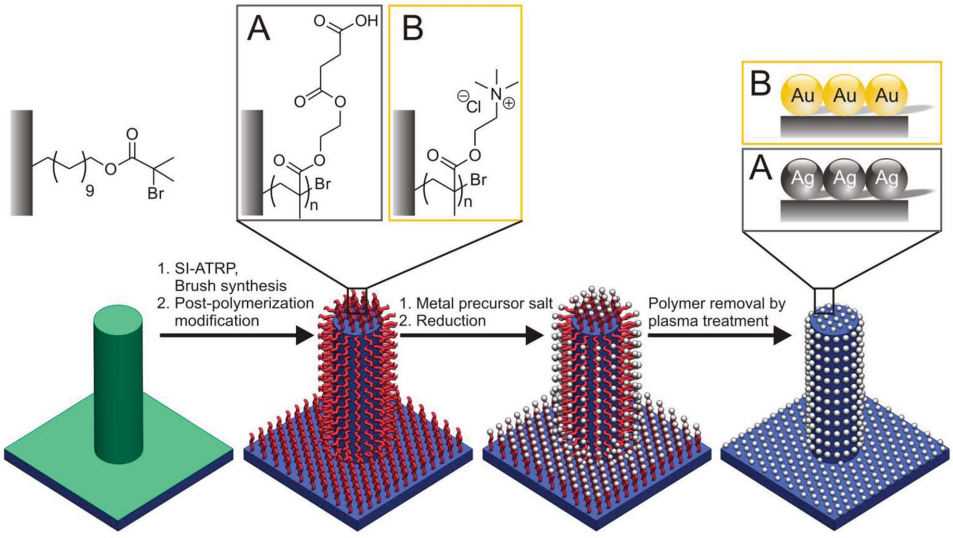

Figure 1. Polymer brush guided preparation of conformal A) silver or B) gold nanoparticle films as top electrode on *pn* junction microwire-based solar cells.

brush films are loaded with an appropriate metal precursor salt followed by a reduction step, which generates a polymer brush metal nanoparticle composite film. In a final step, the stabilizing polymer brush matrix is removed resulting in a thin metal nanoparticle film.

2. Results and Discussion

As a first proof-of-concept, the process outlined in Figure 1 was used to prepare radial *pn* junction planar and microwire-based solar cells with a gold or silver nanoparticle electrode layer. The *p*-core Si microwires were fabricated on a 380 µm thick Czochralski ⟨100⟩ wafer (ρ = 1–10 Ω cm) by a combination of photolithography and deep reactive ion etching as described in a previous report.[28] The diameter, spacing and length of the wires were 2.8, 8, and 9.8 µm, respectively, and the area of the complete devices 16 mm^2. A 450 nm thick *n*-doped shell was formed by diffusion of $POCl_3$ at 850 °C for 35 min. After that, the samples were cleaned by oxygen plasma before removing the native oxide layer with 40% HF. Finally, a layer of 200 nm of Al was sputtered on the back side as a rear contact. The silicon surface of the planar and microwire-based solar cells was modified with undecyl 2-bromo-2-methylpropanoate (see Scheme S1, Supporting Information)[29,30] in order to allow the preparation of the polymer brush template via surface-initiated atom transfer radical polymerization (SI-ATRP). Gold nanoparticle films were prepared following an established protocol[27] using a poly((2-(methacryloyloxy)ethyl)-trimethylammonium chloride) (PMETAC) polymer brush template. Silver nanoparticle electrode coatings were prepared from carboxylic acid functionalized templates, which were obtained via postpolymerization modification of poly(2-hydroxyethyl methacrylate) (PHEMA) brushes with succinic anhydride.[31] The brush coated substrates were subsequently immersed in an aqueous silver nitrate solution and the silver salt reduced with sodium borohydride to generate a polymer brush silver nanoparticle composite film. Finally, hydrogen plasma was applied in order to remove the polymer brush matrix and generate the silver nanoparticle film.[32] As a typical example, **Figure 2** shows scanning electron microscopy (SEM) images of microwires covered with 7, 17, and 24 nm thick silver nanoparticle films. Additional SEM images of silver and gold nanoparticle coated microwires are included in Figures S1 and S2, Supporting Information. The SEM images, and especially those recorded from microwires modified using thick polymer brush templates, reveal that the nanoparticles form clusters that are organized in percolating films that cover the entire surface of the device. The ring-like features around the wires are the result of and typical for the Bosch etching process that is used to create the microwires. The structure of the metal nanoparticle films was further analyzed with atomic force microscopy (AFM). **Figure 3** shows AFM scans of 7, 17, and 24 nm thick silver nanoparticle films, which were obtained from PHEMA brushes with thicknesses of 95, 154, and 276 nm on planar *pn* junction substrates. These AFM images indicate that after removal of the polymer brush matrix the nanoparticles form a dense, percolating film. Further discussion of these AFM analyses will be provided later on in the manuscript (vide infra). Together, the microscopic analyses that are presented in Figures 2 and 3 demonstrate the excellent conformability of the silver nanoparticle film to the

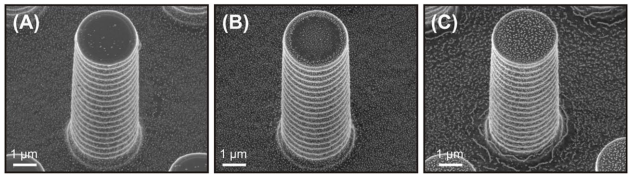

Figure 2. SEM images tilted 25° of microwire-based devices covered by a conformal silver nanoparticle film with a thickness of A) 7, B) 17, and C) 24 nm (reducing agent concentration of 10×10^{-3} M). The silver nanoparticle films in images (A), (B), and (C) were prepared from PHEMA brush templates with thicknesses of 95, 154, and 276 nm, respectively (i.e., polymerization times of 1, 2, and 7 h).

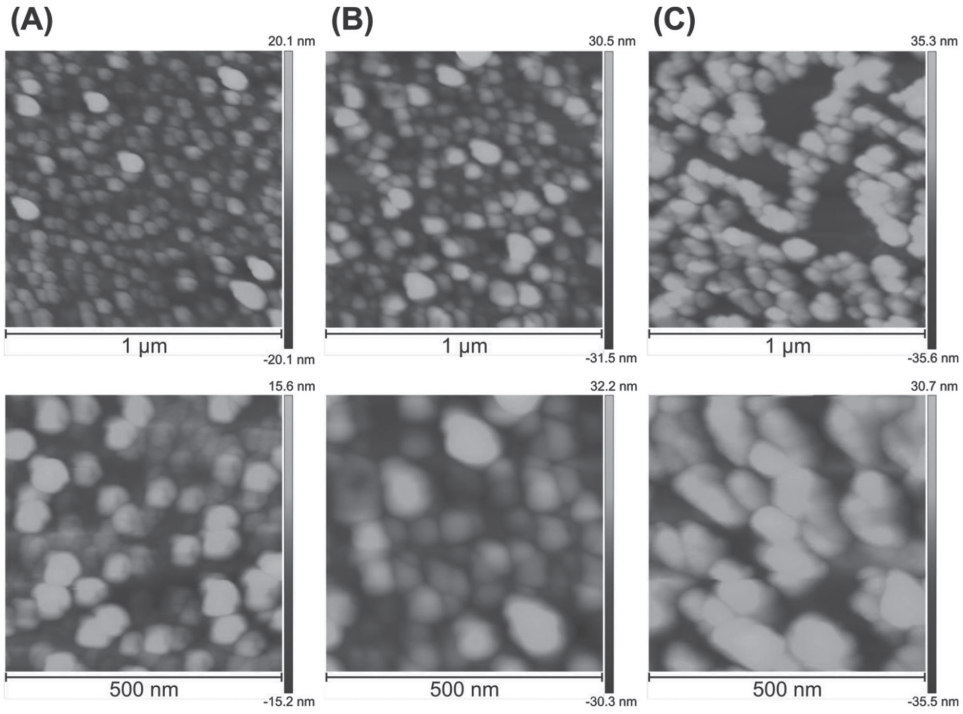

Figure 3. AFM scans of silicon substrates covered with silver nanoparticle films of A) 7 nm, B) 17 nm, and C) 24 nm thickness, which were prepared using a reducing agent concentration of 10×10^{-3} M.

3D microwire surface. In what follows below, we will successively discuss (i) the results of the analyses that were carried out to monitor each of the steps in the fabrication process, and (ii) the photovoltaic characteristics of the metal nanoparticle coated solar cells.

The polymer brush guided formation of the silver and gold nanoparticle films was monitored using a combination of XPS, UV–vis and AFM measurements. All of these experiments were carried out on planar samples, which were taken from the unused area of the wafers employed for the preparation of the microwire arrays, i.e., the part that was not modified with microwires. **Figure 4** and Figure S3, Supporting Information, show the XPS survey spectra and high resolution scans that were recorded at different stages during the fabrication of a silver nanoparticle film. First of all, the XPS spectra demonstrate the successful immobilization of the bromoisobutyrate initiator on the silicon surfaces, as evidenced by the presence of a Br 3d signal at 71.0 eV in the corresponding XPS high-resolution scan (Figure S3, Supporting Information). After SI-ATRP of HEMA, the survey XPS spectrum only reveals the O 1s and C 1s signals indicative of a uniform coverage of the underlying substrate and the C 1s high resolution scan can be deconvoluted in 5 Gaussians in agreement with the chemical composition of the brush (Figure 4A).[33] Postpolymerization modification of the PHEMA brush with succinic anhydride results in an increase in the relative intensity of the carbonyl and ether C 1s signals at 289.1 and 287.0 eV, respectively (Figure S3, Supporting Information). The O 1s signal of the postmodified brush can be deconvoluted in three signals with relative areas of 3:2:1, indicating a quantitative postpolymerization modification of the PHEMA brush with succinic anhydride. Further evidence for the quantitative postpolymerization modification of the PHEMA brush with succinic anhydride was obtained from FTIR analysis (Figure S4, Supporting Information), which revealed a complete disappearance of the hydroxyl band at ≈3400 cm^{-1} upon treatment of the polymer brush film with succinic anhydride. Loading of the carboxylic acid modified polymer films with silver ions by exposure to an aqueous silver nitrate solution was accompanied by the appearance of a Ag 3d doublet at 374.8 (Ag $3d_{3/2}$) and 368.8 (Ag $3d_{5/2}$) (Figure S3, Supporting Information).[34] Subsequent treatment with sodium borohydride to reduce the silver salt and generate the desired silver nanoparticles was accompanied by a shift of the Ag $3d_{3/2}$ and Ag $3d_{5/2}$ peaks to 373.8 and 367.8 eV, respectively, which is in good agreement with the formation of metallic Ag(0) nanoparticles in a polymer brush matrix (Figure 4B).[35] Figure 4C shows the XPS survey spectrum as well as C 1s and Ag 3d high resolution scans after treatment of the polymer brush silver nanoparticle composite film with a hydrogen plasma. The strong decrease in the intensity of the C 1s signal together with the absence of PHEMA characteristic signals are indicative for a complete removal of the stabilizing polymer brush matrix. The remnant C 1s signal is probably due to some residual contaminants. Complete (or near to complete) removal of the polymer brush matrix is also evident from the large decrease in film thickness as monitored by AFM (vide infra, **Figure 5**B). The PMETAC guided formation of gold nanoparticle films was monitored in a similar fashion with XPS. The results are summarized in Figure S5, Supporting Information, but are not discussed in detail since this process was carried out following a previously published procedure.[27]

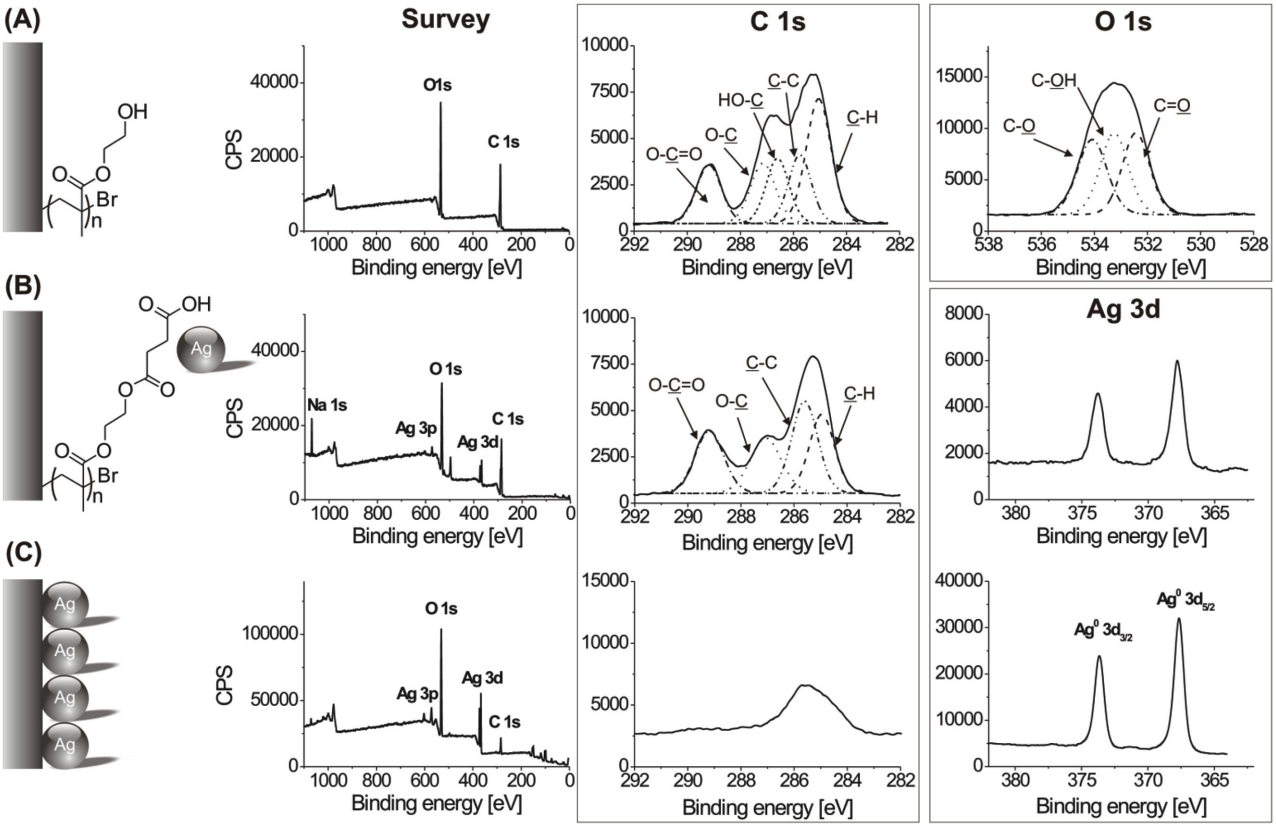

Figure 4. XPS survey and high-resolution C 1s, O 1s, and Ag 3d spectra of *pn* junction silicon substrates modified with A) a 69 nm thick PHEMA brush, B) a 112 nm thick silver nanoparticle polymer brush composite film (prepared using 10×10^{-3} M $NaBH_4$) and C) a 12 nm thick silver nanoparticle film.

The formation of the silver nanoparticles can also be monitored using UV–vis spectroscopy. To this end, the method presented in Figure 1 was used to deposit thin silver and gold nanoparticle films on glass substrates. The successful reduction of the polymer brush entrapped silver salt and the concomitant generation of the silver nanoparticles is characterized by the appearance of the typical plasmon absorbance around ≈420 nm (Figure 5A). Peak plasmon resonance wavelengths around ≈420 nm have been assigned to spherical silver nanoparticles with a diameter of ≈40–50 nm.[36] When the thickness of the polymer brush template increases, the absorbance at 420 nm increases. This reflects the enhanced precursor salt loading capacity and as a consequence the increase in silver nanoparticle film thickness as the brush thickness increases (Figure 5C). Upon decreasing the concentration of the reducing agent from 100 to 10 to 1×10^{-3} M, a red-shift of the silver plasmon absorption to 470 nm was observed, which could be due to an increase in size of the silver nanoparticles or due to

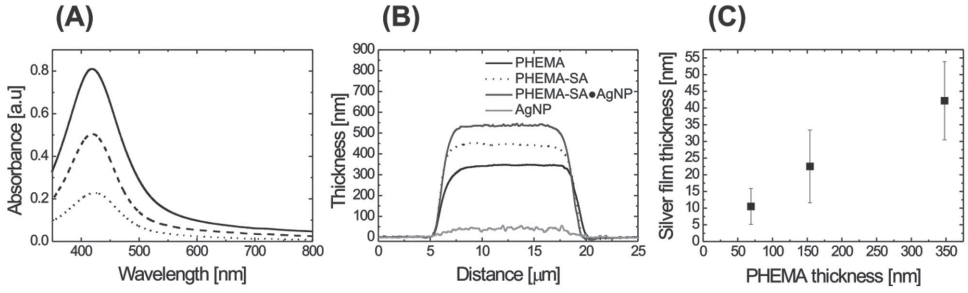

Figure 5. A) UV–vis spectra of silver nanoparticle PHEMA composite films prepared from PHEMA brushes with thicknesses of 95 nm (dotted line), 151 nm (dashed line), and 276 nm (solid line). The films were prepared on planar glass substrates and obtained after reduction of $AgNO_3$ loaded precursor polymer brushes with 10×10^{-3} M $NaBH_4$. B) AFM cross-sectional profiles of a patterned PHEMA brush (black), a carboxylic acid postmodified PHEMA brush (PHEMA-SA) (dotted line), a PHEMA brush–silver nanoparticle composite film (PHEMA-SA·AgNP) obtained after reduction of the corresponding silver salt loaded precursor with 10×10^{-3} M $NaBH_4$ (blue) and a silver nanoparticle film (AgNP) after hydrogen plasma removal of the polymer brush matrix (green). C) Comparison of the silver nanoparticle film thickness obtained after plasma treatment of the PHEMA brush–silver nanoparticle composite film with that of the initial PHEMA brush template.

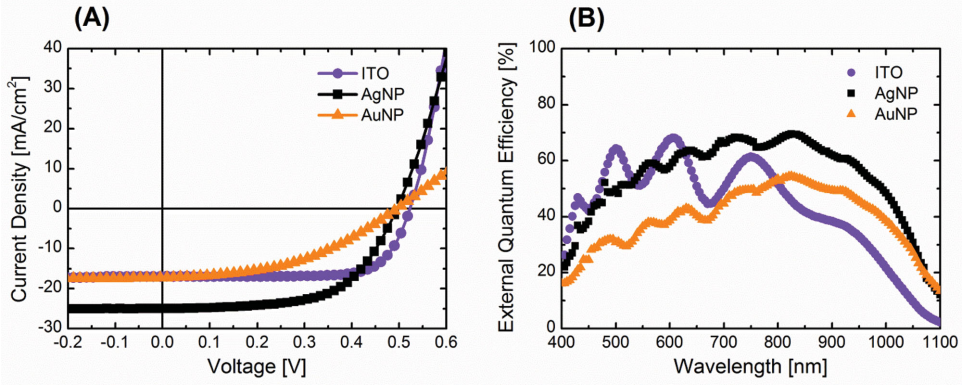

Figure 6. Comparison of planar Si solar cells coated with three different front electrodes: (■) a 17 nm thick silver nanoparticle film, (▲) a 75 nm thick gold nanoparticle film, and (●) a 200 nm thick sputtered ITO: A) *J–V* curves under an illumination of AM 1.5 G and B) EQE of the three devices.

partial aggregation of the silver nanoparticles in the polymer brush matrix (Figure S6, Supporting Information).[37] UV–vis spectra of $HAuCl_4$ loaded PMETAC brushes as well as the corresponding polymer brush gold nanoparticle composite films and the final gold nanoparticle films are included in Figure S7 in the Supporting Information.

Figure 5B shows AFM cross-sectional profiles recorded on planar micropatterned *pn* junction substrates at various steps during the preparation of a silver nanoparticle coating. Post-polymerization modification of a PHEMA brush with an initial thickness of 345 nm with succinic anhydride results in an increase of film thickness to 447 nm. Loading with the silver precursor salt and subsequent reduction leads to a polymer brush silver nanoparticle composite film with a thickness of 536 nm. Finally, hydrogen plasma treatment to remove the brush matrix generates a silver nanoparticle film with a thickness of 42 nm. As illustrated in Figure 5C, the thickness of the final silver nanoparticle film can be modulated by varying the thickness of the PHEMA brush-based template. Further insight into the structure of the silver nanoparticle films can be obtained from the AFM scans and cross-sectional profiles that are included in Figure 3 and Figure S8, Supporting Information. These analyses show that the silver nanoparticles form a percolating mesh on top of the silicon surface, which allows transport of charge carriers and simultaneously enables photons to reach the silicon surface. Particle size analysis of the images in Figure 3 reveals particle diameters of 68 ± 40, 74 ± 43, and 54 ± 34 nm for the images in Figure 3A–C, respectively. These particles sizes agree relatively well with the location of the peak plasmon wavelength (≈420 nm (Figure 5A), $d_{\text{nanoparticle}}$ = 40–50 nm, vide supra). There is no significant difference in particle size which is due to the fact that the films have been prepared using the same concentration of $NaBH_4$ in the reduction step. The relatively large standard deviations in the particle size reflect the aggregation of the nanoparticles. AFM characterization results of the different steps in the PMETAC directed formation of gold nanoparticle films are provided in the Supporting Information (Figure S9, Supporting Information).

As a first assessment of the potential of the polymer brush templated metal nanoparticle films to act as front electrodes, the performance of planar cells coated with 75 nm thick gold and 17 nm thick silver nanoparticle films were compared to the same device coated with a 200 nm thick layer of sputtered ITO (ρ = 0.2 mΩ cm). Their *J–V* curves together with the main parameters extracted from these measurements are shown in **Figure 6**A and **Table 1**, respectively. Figure S10, Supporting Information, compares the photovoltaic properties of ITO and silver and gold nanoparticle coated planar Si solar cells with those of an unmodified device, i.e., a planar Si substrate without a top electrode.

The data summarized in Table 1 and Figure 6 provide first insight into the photovoltaic properties of the nanoparticle electrode coated planar Si solar cells. First, it can be seen that the series resistance of the silver nanoparticle coated cell (R_s = 12 Ω) is slightly higher than that of standard ITO (R_s = 3 Ω). On the contrary, the gold nanoparticle film is much more resistive (R_s = 80 Ω), which may be attributed to a (combination of a) higher Schottky barrier at the Au/*n*-Si interface and/or the morphology of the gold nanoparticle film. In addition, whereas the gold nanoparticle electrode film shows a short circuit current density (J_{sc}) comparable to that of the ITO cell, J_{sc} is increased by 46% for the silver nanoparticle-based device. The increased J_{sc} indicates a higher light absorption by the silver nanoparticle modified device as compared to the ITO coated counterpart. The enhanced light absorption of the metal nanoparticle films is also reflected in the results of external quantum efficiency (EQE) measurements, which are presented in Figure 6B. Both metal nanoparticle electrode films exhibit a higher EQE at long wavelengths than the ITO device. As the optical transparency of the ITO electrode is much better than that of the gold and silver nanoparticle electrodes (see Figure S11, Supporting Information), this is attributed to scattering by the plasmonic nanoparticles.[19,38–40] The coefficient of absorption of silicon in the longer wavelengths is small because it is an indirect bandgap

Table 1. Photovoltaic characteristics of planar solar cells coated with different front electrode films.

Electrode material	Film thickness [nm]	J_{sc} [mA cm^{-2}]	V_{oc} [V]	FF	R_s [Ω]	η [%]
Ag	17	24.9	0.50	0.60	12	7.4
Au	75	17.3	0.50	0.44	80	3.8
ITO	200	17.0	0.52	0.74	3	6.6

semiconductor. The metallic nanoparticles scatter the light and thereby change the direction of propagation, meaning that light can stay in the micropillars by multiple reflections on the facets. This allows a better absorption and collection of the photogenerated carriers. The overall efficiency (η) of the silver nanoparticle-based solar cell is 7.4%, as compared to 6.6% for the ITO coated device and 3.8% for the gold nanoparticle device. These differences may be due to a number of parameters including the work function of the different materials, the plasmonic properties of the metal nanoparticles as well as the morphology of the metal nanoparticle film. The results in Figure S10, Supporting Information, indicate that even though the conductivity of the *n*-Si is quite high (R_s = 28 Ω), the absence of an electrode hinders the extraction of carriers, resulting in low FF and shunt resistance (R_p). This demonstrates that the metal nanoparticle films act as an electrode and facilitate carrier extraction. This is consistent with the SEM and AFM analyses that were presented in Figures 2 and 3, which indicated that the metal nanoparticles form dense, interconnected and percolating networks. Ongoing experiments are focusing on deciphering the influence of the type of nanoparticle and film micro/nanostructure on the properties of the electrode layers. While the process developed in this manuscript is of most interest for the modification of complex, structured solar cell substrates with an electrode layer, comparing planar solar cells with the nanoparticle-based electrodes and ITO is valuable as it provides fundamental insights in the properties of these new electrode materials.

As a final proof-of-concept, microwire solar cells were coated with a silver nanoparticle electrode film. Typical *J*–*V* characteristics of a silver nanoparticle coated microwire-based device and its planar counterpart under AM 1.5 G illumination are presented in **Figure 7**, showing a typical diode behavior. The device has a R_s of 16 Ω, an open-circuit voltage (V_{oc}) of 0.35 V, a fill factor (FF) of 0.36, a J_{sc} of 22.7 mA cm^{-2} and an efficiency (η) calculated over the total projected area of 2.8%. The J_{sc} of the microwire cell is very close to that of the planar counterpart. The FF and V_{oc} values of the microwire-based device are much lower than those of the planar cell. This could be attributed to Ohmic losses at the metal/Si interface, which are more significant for the microwire-based devices as they have a much higher surface-to-volume ratio as compared to the planar solar cells. The series resistance of the microwire-based devices, however, is still higher as compared to that of the corresponding planar Si solar cells presented above. This reduces the fill factor of the device and thereby the efficiency. Ongoing work focuses on optimization of the electrical properties for the improvement of the fill factor of the devices.

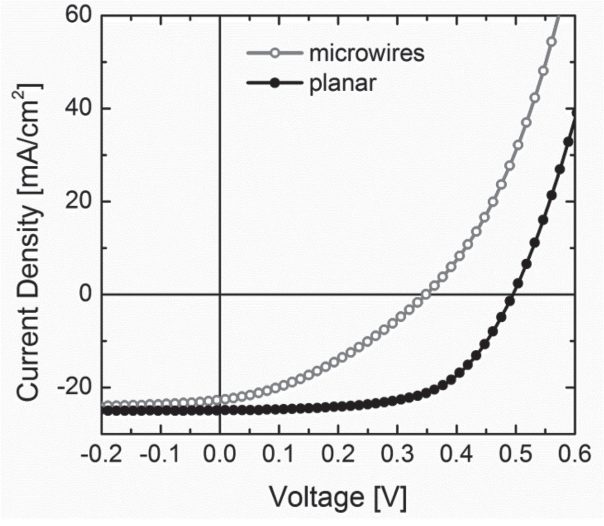

Figure 7. *J*–*V* characteristics of the best planar and microwire-based solar cells under AM 1.5 G illumination. The thickness of the silver nanoparticle film is 17 nm in both cases.

Table 2. Photovoltaic properties of microwire solar cells coated with silver nanoparticle films of different thicknesses.

Film thickness [nm]	J_{sc} [mA cm^{-2}]	V_{oc} [V]	FF	R_s [Ω]	η [%]
7	17.8	0.38	0.29	143	2.0
17	22.7	0.35	0.36	16	2.8
24	23.6	0.30	0.36	14	2.5

The effect of the thickness of the silver nanoparticle electrode film on the device characteristics was also investigated. By varying the initial thickness of the PHEMA brush, silver nanoparticle electrode coatings with thicknesses of 7, 17, and 24 nm were obtained using a reducing agent concentration of 10×10^{-3} M. The photovoltaic properties of microwire-based devices coated with these three different film thicknesses are summarized in **Table 2**.

Increasing the silver nanoparticle film thickness from 7 to 17 to 24 nm results in a decrease in R_s and, as a consequence, an increase in conductivity. In addition, J_{sc} also increases with the thickness, exhibiting an increment of 27.5% and 32.6% for the 17 and 24 nm thick films with respect to the film of 7 nm, respectively. The overall efficiency of the different microwire solar cells varies between 2.0% and 2.8% depending on the thickness of the silver nanoparticle coating. In a first instance, the increase in J_{sc} that is observed upon increasing the film thickness from 7 to 17 and 24 nm may be attributed to the larger number of plasmonic scattering centers that constitute the thicker films. In principle, electrode coatings composed of densely packed arrays of relatively large silver nanoparticles, would be beneficial to further enhance the device performance as they would enhance scattering cross section over extinction cross section.[19,40,41] Further improving the performance of the microwire-based solar cells involves optimization of the amount of nanoparticles on the nanowire surface (which correlates with the thickness of the sacrificial polymer brush layer) to maximize electron transport and light scattering as well as transmission through the electrode. Such an optimization requires an optimization algorithm and is the subject of ongoing work.

3. Conclusions

In conclusion, we have presented a novel process for the modification of silicon microwire-based solar cells with a conformal, percolating metal nanoparticle-based electrode. The proposed strategy is based on the use of a sacrificial thin polymer coating

("polymer brush") that acts as a template to guide the formation of the metal nanoparticle electrode layer. The resulting metal nanoparticle films are unique in that they perform a dual function by simultaneously acting as an electrode that can mediate charge transport and enhance light capture due to the plasmonic scattering properties of the metal nanoparticles. Coating a planar silicon solar cell with a 17 nm thick silver nanoparticle electrode results in a device with a J_{sc} of 24.9 mA cm^{-2} and an efficiency of 7.4% as compared to a J_{sc} of 17.0 mA cm^{-2} and an efficiency of 6.6% for the corresponding ITO coated device, which underlines the attractiveness of these metal nanoparticle electrode coatings as an alternative to classical electrode materials.

4. Experimental Section

Materials: 2-Hydroxyethyl methacrylate (HEMA) and *N,N*-dimethylaminoethyl methacrylate (DMAEMA) were obtained from Aldrich and freed from the inhibitor by passing the monomer through a column of activated basic aluminium oxide. 2,2′-Bipyridine (bipy), $CuBr_2$ (99.999%), CuCl (purum, ≥ 99.995%), CuBr (purum, ≥99,99%), Pt/C (10% Pt), iodomethane (99%), 2-bromo-2-methylpropionyl bromide (98%), dimethylchlorosilane (98%), 5-hexen-1-ol, NaCl, gold(III) chloride hydrate ($HAuCl_4$ > 52% Au, ACS grade), sodium borohydride (99%), 4-(dimethylamino)pyridine (DMAP), succinic anhydride (SA), hydrofluoric acid (40%), 10-undecylenic acid methyl ester (96%), lithium aluminium hydride (powder, 95%), and silver nitrate (ACS reagent, ≥99%) were purchased from Aldrich and used as received. Triethylamine (Et_3N) was purchased from Aldrich and was distilled over KOH before use. Tetrahydrofurane (THF), dichloromethane and toluene were purified and dried using a solvent purification system (PureSolv). Deionized water was obtained from a Millipore Direct-Q 5 Ultrapure Water System. 6-(Chlorodimethylsilyl)hexyl 2-bromo-2-methylpropanoate was synthesized as described previously.[42]

Analytical Methods: X-ray photoelectron spectroscopy was carried out using an Axis Ultra instrument from Kratos Analytical equipped with a conventional hemispheric analyzer. The X-ray source employed was a monochromatic Al Kα (1486.6 eV) source operated at 100 W and 10^{-9} mbar. All XPS spectra were calibrated on the aliphatic carbon signal at 285.0 eV. Water contact angles were determined using a DataPhysics OCA 35 contact angle measurement instrument. ^{1}H and ^{13}C NMR spectra were recorded on a Bruker AVANCE-400 Ultra Shield spectrometer. Chemical shifts are reported in parts per million (ppm) using the residual solvent peak as internal standard. Atomic force microscopy was performed on a Veeco Multimode Nanoscope IIIa SPM controller (Digital Instruments, Santa Barbara, CA) in tapping mode using NSC14/AIBS or NSC15/noAl Mikromash (Tallinn, Estonia) cantilevers. Polymer brush thicknesses were determined under ambient conditions by AFM using micropatterned polymer brushes as described previously.[25] Optical micrographs were taken with an Olympus BH2 optical microscope. The substrates were cleaned before any functionalization using a Tepla 300 microwave induced plasma system (PVA Tepla AG, Germany) during 4 min at 500 W with an oxygen flow rate of 400 mL min^{-1}.

Procedure: Preparation of Gold Nanoparticle Films: Surface modification of silicon substrates (planar, microwire arrays, and Pyrex samples) with gold nanoparticle films was performed as reported previously.[27] Polymer brush substrates loaded with gold nanoparticles were exposed to oxidative plasma using a Tepla 300 microwave in order to remove the polymer template. Samples were subjected to 4 cycles of plasma treatment as described above.

Modification of Silicon Substrates with the ATRP Initiator: Previous to any surface modification, substrates were first cleaned under ultrasound in ethanol, water, and acetone (5 min each) and then later by oxygen plasma during 10 min. The native oxide layer of the silicon oxide and *pn* junction microwire array substrates was first removed by immersing them in a 40% hydrofluoric acid for 5 min (**Caution!** *HF is extremely dangerous and must be handled with appropriate precautions*). The substrates were extensively cleaned with dichloromethane, dried and directly used. UV-induced coupling with 10-undecylenic acid methyl ester (UAME) was performed as described in ref. [30]. A few drops of UAME were placed on the substrates, which were subsequently covered with a Pyrex plate and exposed to UV light during 30 min. After the coupling, the substrates were thoroughly washed with acetone and dried overnight under vacuum. The reduction of the ester was carried out as followed; 1.6 g of $LiAlH_4$ was added slowly under nitrogen to 33 mL of dry THF in a 100 mL Schlenk tube. The reaction mixture was then transferred under nitrogen to a reactor containing the substrates and the reduction was allowed to proceed for 4 h at room temperature. The obtained modified surfaces were removed from the reaction mixture and washed thoroughly with acetone, 0.5 M HCl solution, acetone and water. Samples were dried under a flow of nitrogen and later overnight under the vacuum. Esterification proceeded at 0 °C by immersing the substrates into a solution of Et_3N (0.23 mL, 1.65 mmol, 55×10^{-3} M) and DMAP (201.58 mg, 1.65 mmol, 55×10^{-3} M) in 30 mL dry THF to which a mixture of 2-bromo-2-methylpropionyl bromide (0.185 mL, 1.5 mmol, 50×10^{-3} M) diluted in 5 mL of dry THF was added dropwise under stirring. The reaction proceeded 2 h at 0 °C and was subsequently left for 10 h at room temperature. Samples were washed with THF, ethanol, water, and ethanol and dried over nitrogen. The samples were then kept under vacuum and used directly for polymerization.

Synthesis of Succinic Anhydride-Postmodified PHEMA Brushes: The preparation of PHEMA brushes via SI-ATRP and the subsequent postpolymerization modification with succinic anhydride were carried out following established protocols.[31]

Preparation of Silver Nanoparticle Films: After extensive cleaning with THF, ethanol, water, and ethanol, the postmodified substrates were dried under nitrogen and immersed overnight in a 10×10^{-3} M aqueous solution of silver nitrate. The samples were then thoroughly washed with water and dried before reduction of the films. Reduction was carried out during 30 sec using a fresh aqueous sodium borohydride solution with concentrations of 1×10^{-3}, 10×10^{-3}, and 100×10^{-3} M. The samples were rinsed with water and dried under a nitrogen flow. At last, the samples were exposed to reducing plasma to afford the silver nanoparticle films. A reducing plasma was applied to the polymer brush silver nanoparticle composite film covered substrates using a 9:1 mixture of Argon and hydrogen in a homemade plasma chamber at a constant pressure (0.500 mbar) during 10 min at 300 W.

Supporting Information

Supporting Information is available from the Wiley Online Library or from the author.

Acknowledgements

C.S. and A.D.M. contributed equally to this work. C.S. and H.-A.K acknowledge support by the Precision Polymer Materials (P2M) Research Networking Programme of the European Science Foundation (ESF). A.D.M and A.F.i M. acknowledge funding through ERC Stg UpCon and NanoTera project Synergy. The authors are grateful to N. Leiser and L.-M. Genoud (Institute of Condensed Matter Physics (ICMP), EPFL) for their help with the hydrogen plasma experiments and to S. Desseaux for her help with analyzing the AFM images.

Received: November 29, 2014
Revised: April 27, 2015
Published online: May 22, 2015

[1] C. Battaglia, J. Escarré, K. Söderström, M. Charrière, M. Despeisse, F.-J. Haug, C. Ballif, *Nat. Photonics* **2011**, *5*, 535.
[2] E. L. Warren, H. A. Atwater, N. S. Lewis, *J. Phys. Chem C* **2014**, *118*, 747.
[3] K. T. Fountaine, C. G. Kendall, H. A. Atwater, *Opt. Express* **2014**, *22*, A930.
[4] D. M. Callahan, J. N. Munday, H. A. Atwater, *Nano Lett.* **2012**, *12*, 214.
[5] E. D. Kosten, E. L. Warren, H. A. Atwater, *Opt. Express* **2011**, *19*, 3316.
[6] P. Krogstrup, H. I. Jørgensen, M. Heiss, O. Demichel, J. V. Holm, M. Aagesen, J. Nygard, A. Fontcuberta i Morral, *Nat. Photonics* **2013**, *7*, 306.
[7] J. Wallentin, N. Anttu, D. Asoli, M. Huffman, I. Åberg, M. H. Magnusson, G. Siefer, P. Fuss-Kailuweit, F. Dimroth, B. Witzigmann, H. Q. Xu, L. Samuelson, K. Deppert, M. T. Borgström, *Science* **2013**, *339*, 1057.
[8] Z. Fan, D. Ruebusch, A. Rathore, R. Kapadia, O. Ergen, P. Leu, A. Javey, *Nano Res.* **2009**, *2*, 829.
[9] H. Park, J. A. Rowehl, K. K. Kim, V. Bulovic, J. Kong, *Nanotechnology* **2010**, *21*, 505204.
[10] A. D. Pasquier, H. E. Unalan, A. Kanwal, S. Miller, M. Chhowalla, *Appl. Phys. Lett.* **2005**, *87*, 203511.
[11] Z. Wu, Z. Chen, X. Du, J. Logan, J. Sippel, M. Nikolou, K. Kamaras, J. R. Reynolds, D. B. Tanner, A. F. Hebard, A. G. Rinzler, *Science* **2004**, *305*, 1273.
[12] G. P. Kushto, W. Kim, Z. H. Kafafi, *Appl. Phys. Lett.* **2005**, *86*, 093502.
[13] Y. Zhou, F. Zhang, K. Tvingstedt, S. Barrau, F. Li, W. Tian, O. Inganas, *Appl. Phys. Lett.* **2008**, *92*, 233308.
[14] L. Hu, G. Zheng, J. Yao, N. Liu, B. Weil, M. Eskilsson, E. Karabulut, Z. Ruan, S. Fan, J. T. Bloking, M. D. McGehee, L. Wagberg, Y. Cui, *Energy Environ. Sci.* **2013**, *6*, 513.
[15] S. De, T. M. Higgins, P. E. Lyons, E. M. Doherty, P. N. Nirmalraj, W. J. Blau, J. J. Boland, J. N. Coleman, *ACS Nano* **2009**, *3*, 1767.
[16] J.-Y. Lee, S. T. Connor, Y. Cui, P. Peumans, *Nano Lett.* **2008**, *8*, 689.
[17] H. Wu, D. Kong, Z. Ruan, P.-C. Hsu, S. Wang, Z. Yu, T. J. Carney, L. Hu, S. Fan, Y. Cui, *Nat. Nanotechnol.* **2013**, *8*, 421.
[18] J. van de Groep, P. Spinelli, A. Polman, *Nano Lett.* **2012**, *12*, 3138.
[19] H. A. Atwater, A. Polman, *Nat. Mater.* **2010**, *9*, 205.
[20] K. R. Catchpole, A. Polman, *Appl. Phys. Lett.* **2008**, *93*, 191113.
[21] M. J. Mendes, I. Tobías, A. Martí, A. Luque, *Opt. Express* **2011**, *19*, 16207.
[22] R. Barbey, L. Lavanant, D. Paripovic, N. Schüwer, C. Sugnaux, S. Tugulu, H.-A. Klok, *Chem. Rev.* **2009**, *109*, 5437.
[23] D. J. Kim, K.-B. Lee, Y. S. Chi, W.-J. Kim, H.-j. Paik, I. S. Choi, *Langmuir* **2004**, *20*, 7904.
[24] D. J. Kim, K.-B. Lee, T. G. Lee, H. K. Shon, W.-J. Kim, H.-J. Paik, I. S. Choi, *Small* **2005**, *1*, 992.
[25] S. Tugulu, M. Harms, M. Fricke, D. Volkmer, H.-A. Klok, *Angew. Chem., Int. Ed.* **2006**, *45*, 7458.
[26] S. H. Yang, K. Kang, I. S. Choi, *Chem. Asian J.* **2008**, *3*, 2097.
[27] D. Paripovic, H.-A. Klok, *ACS Appl. Mater. Interfaces* **2011**, *3*, 910.
[28] A. Dalmau Mallorquí, F. M. Epple, D. Fan, O. Demichel, A. Fontcuberta i Morral, *Phys. Status Solidi A* **2012**, *209*, 1588.
[29] X. Wang, R. E. Ruther, J. A. Streifer, R. J. Hamers, *J. Am. Chem. Soc.* **2010**, *132*, 4048.
[30] D. Xu, W. H. Yu, E. T. Kang, K. G. Neoh, *J. Colloid Interface Sci.* **2004**, *279*, 78.
[31] C. Sugnaux, L. Lavanant, H.-A. Klok, *Langmuir* **2013**, *29*, 7325.
[32] G. Kästle, H. G. Boyen, F. Weigl, G. Lengl, T. Herzog, P. Ziemann, S. Riethmüller, O. Mayer, C. Hartmann, J. P. Spatz, M. Möller, M. Ozawa, F. Banhart, M. G. Garnier, P. Oelhafen, *Adv. Funct. Mater.* **2003**, *13*, 853.
[33] J. F. Watts, *Surf. Interface Anal.* **1993**, *20*, 267.
[34] A. M. Ferraria, A. P. Carapeto, A. M. Botelho do Rego, *Vacuum* **2012**, *86*, 1988.
[35] D. Dasgupta, I. K. Shishmanova, A. Ruiz-Carretero, K. Lu, M. Verhoeven, H. P. C. van Kuringen, G. Portale, P. Leclère, C. W. M. Bastiaansen, D. J. Broer, A. P. H. J. Schenning, *J. Am. Chem. Soc.* **2013**, *135*, 10922.
[36] J. J. Mock, M. Barbic, D. R. Smith, D. A. Schultz, S. Schultz, *J. Chem. Phys.* **2002**, *116*, 6755.
[37] E. M. Benetti, X. Sui, S. Zapotoczny, G. J. Vancso, *Adv. Funct. Mater.* **2010**, *20*, 939.
[38] F. J. Beck, E. Verhagen, S. Mokkapati, A. Polman, K. R. Catchpole, *Opt. Express* **2011**, *19*, A146.
[39] S. Pillai, K. R. Catchpole, T. Trupke, M. A. Green, *J. Appl. Phys.* **2007**, *101*, 093105.
[40] K. R. Catchpole, A. Polman, *Opt. Express* **2008**, *16*, 21793.
[41] P. G. Kik, M. L. Brongersma, in *Surface Plasmon Nanophotonics*, Vol. *131* (Eds: M. L. Brongersma, P. G. Kik) Springer, Berlin **2007**, pp. 1–9.
[42] N. Schüwer, H.-A. Klok, *Adv. Mater.* **2010**, *22*, 3251.